

Development and Simulation of Sulfur-doped Graphene Supported Platinum with Exemplary Stability and Activity Towards Oxygen Reduction

Drew Higgins, Md Ariful Hoque, Min Ho Seo, Rongyue Wang, Fathy Hassan, Ja-Yeon Choi, Mark Pritzker, Aiping Yu, Jiujun Zhang, and Zhongwei Chen*

Sulfur-doped graphene (SG) is prepared by a thermal shock/quench anneal process and investigated as a unique Pt nanoparticle support (Pt/SG) for the oxygen reduction reaction (ORR). Particularly, SG is found to induce highly favorable catalyst-support interactions, resulting in excellent half-cell based ORR activity of 139 mA mg_{Pt}⁻¹ at 0.9 V vs RHE, significant improvements over commercial Pt/C (121 mA mg_{Pt}⁻¹) and Pt-graphene (Pt/G, 101 mA mg_{Pt}⁻¹). Pt/SG also demonstrates unprecedented stability, maintaining 87% of its electrochemically active surface area following accelerated degradation testing. Furthermore, a majority of ORR activity is maintained, providing 108 mA mg_{Pt}⁻¹, a remarkable 171% improvement over Pt/C (39.8 mA mg_{Pt}⁻¹) and an 89% improvement over Pt/G (57.0 mA mg_{Pt}⁻¹). Computational simulations highlight that the interactions between Pt and graphene are enhanced significantly by sulfur doping, leading to a tethering effect that can explain the outstanding electrochemical stability. Furthermore, sulfur dopants result in a downshift of the platinum d-band center, explaining the excellent ORR activity and rendering SG as a new and highly promising class of catalyst supports for electrochemical energy technologies such as fuel cells.

1. Introduction

Polymer electrolyte membrane fuel cells (PEMFCs) offer the unanimous appeal of high energy conversion efficiencies, excellent energy densities and environmentally benign operation; however require highly active and operationally stable catalysts to facilitate the inherently sluggish oxygen reduction

reaction (ORR) occurring at the cathode. Conventional PEMFC systems employ platinum (Pt) based catalysts, which to date have been the only materials capable of facilitating the ORR at rates practical, although still insufficient for PEMFC operation. The widespread commercialization and deployment of PEMFCs into advanced sustainable energy infrastructures including the automotive sector is still limited by three primary factors: i) high cost, ii) insufficient performance, and iii) low durability.^[1,2] At the root of these limitations lies the aforementioned expensive Pt catalyst materials employed; generally consisting of Pt nanoparticles ($\approx 2\text{--}3$ nm) uniformly distributed on high surface area carbon black supports (Pt/C).

Although significant improvements to state-of-the-art Pt/C catalysts and electrode designs for automobile PEMFCs has been realized in recent years, an immense challenge in achieving the 2017 technical

targets set by the United States Department of Energy still remains at the current state of catalyst technology. The targets state that by 2017, the total Pt loading (anode and cathode) must be reduced to below 0.125 mg cm⁻² coupled with 5000 h of operational stability under simulated drive cycles.^[3] Specifically, Pt/C is known to degrade under the harsh oxidizing conditions encountered at the PEMFC cathode due to corrosion of the carbon support materials, or by agglomeration and/or dissolution of the platinum nanoparticles resulting from weak interactions with the catalyst supports.^[4] This in turn leads to a sharp loss in available electrochemically active surface areas (ECSA) and by extension fuel cell performance.

A common approach to improve catalyst stability and activity has involved the design of non-conventional catalyst supports, including transition metal oxides and nitrides;^[5–8] or alternative carbon supports doped with heteroatoms such as nitrogen to enhance the interaction and synergy between the catalyst particle and its support.^[9,10] It is well understood that the structure and properties of the support materials will directly govern the performance and stability of the catalyst materials. There still however remains a lack of fundamental understanding regarding the exact nature of these particular catalyst-support

D. Higgins, M. A. Hoque, Dr. M. H. Seo, Dr. R. Wang, Dr. F. Hassan, J.-Y. Choi, Prof. M. Pritzker, Prof. A. Yu, Prof. Z. Chen

Department of Chemical Engineering
Waterloo Institute for Nanotechnology
Waterloo Institute of Sustainable Energy
University of Waterloo, 200 University Ave. W
Waterloo, ON N2L 3G1, Canada
E-mail: zhwchen@uwaterloo.ca

Dr. J. Zhang
NRC Energy, Mining & Environment
National Research Council Canada, 4250 Wesbrook Mall
Vancouver, BC V6T 1W5, Canada



DOI: 10.1002/adfm.201400161

interactions;^[11] a phenomena that has widespread application in many fields of heterogeneous catalysis.^[12] Recent advances in density functional theory and computational chemistry have now provided us the tools to adequately model catalyst behavior and provide advanced understanding towards electro-catalysis; including the specific catalyst-support interactions occurring at the cathode of fuel cells. It is thereby a worthwhile approach to couple fundamental computational simulations with experimental investigations for uniquely designed novel nanostructured support materials. This will allow scientists to predict, understand and explain support dependent improvements in catalytic activity and durability, thereby providing valuable guidance for future catalyst design endeavors.

Graphene has recently emerged as a highly promising catalyst support material for PEMFC applications owing to its immense surface areas, along with excellent conductivity and electron transfer capabilities that are important criteria pertaining to electro-catalysis.^[13–15] Graphene is theoretically composed of only graphitic carbon atoms which can provide added resilience against carbon corrosion during PEMFC operation,^[16] although the relatively inert and hydrophobic nature of its surface does not culminate in facile Pt deposition, requiring functionalization procedures to obtain well dispersed nanoparticles and overcome stability limitations.^[17] To this end, nitrogen doped graphene and other graphitic carbons have been extensively developed and investigated for fuel cell catalyst applications, either as stand-alone ORR electrocatalysts in alkaline media^[18–26] or as Pt nanoparticle supports under acidic (i.e., PEMFC) conditions.^[27–33] The presence of nitrogen dopants has been reported to exert a “tethering” effect on Pt nanoparticles,^[9,33] providing both beneficial catalyst activity and stability enhancements. While density functional theory simulations exist in the literature investigating the adsorption and binding interactions between Pt and either nitrogen and boron doped graphene or CNTs,^[34–37] there exists an overall lack of fundamental understanding regarding the Pt-heteroatom doped graphene catalyst-support interactions and their associated impact on ORR performance and operational stability. Furthermore, the impact of graphene doped with various other heteroatoms (i.e., sulfur) remains largely unexplored despite their high potential for applications as ORR catalysts^[38–40] or catalyst support materials.^[41] Elucidation of these important considerations can be provided by effectively linking fundamental computational simulations with detailed experimental investigations.

In the present work, we report the development of sulfur-doped graphene (SG) by thermal shock/quench annealing a mixture of graphene oxide (GO) and phenyl disulfide (PDS). These materials were used as Pt nanoparticle support materials, whereby after Pt deposition onto SG (Pt/SG) by a modified ethylene glycol (EG) method, uniformly sized nanoparticles well dispersed across the entirety of the SG surface were successfully obtained. Improved ORR activity was found for Pt/SG in comparison to Pt supported on un-doped graphene (Pt/G) along with commercial state of the art Pt/C. Furthermore and most notably, we also observed significantly enhanced stability of Pt/SG; including excellent ORR activity and ECSA retention after exposing the catalysts to repetitive potential cycles in 0.1 M HClO₄ electrolyte.

On the basis of these observations, we performed ab initio density functional theory calculations to investigate the interactions occurring between SG and Pt and elucidate the root causes of ORR performance and stability enhancements. We found that the strengthened interaction and binding energies between Pt and SG arose, and could exclusively be linked to sulfur incorporation based on comparative investigations with un-doped G. Specifically, sulfur doping led to stronger adsorptive and cohesive binding energies with Pt, leading to the aforementioned catalyst-support tethering effect, along with negatively shifting the d-band center of the Pt atoms. These findings were used to explain the dramatically enhanced stability and improved activity of Pt/SG, respectively, in comparison to both Pt/G and Pt/C. This work represents the first comprehensive report of fundamental ab initio simulations linked to rigorous experimental investigations for sulfur doped graphene, and furthermore Pt/SG is presented for the first time as a highly active ORR catalyst material with exemplary stability capabilities for PEMFC applications.

2. Results and Discussion

2.1. Physicochemical Characterization

After preparation, both SG and G demonstrated a wrinkled voile-like structure consisting of thin single or multi-layer graphene sheets (Figure S1, Supporting Information) and indicative that the presence of PDS during high temperature thermal annealing had negligible impact on the resultant physical structures. With the whole preparation processes schematically depicted in Figure S2 (Supporting Information), Pt nanoparticle deposition by the well-established ethylene glycol technique^[29,42,43] was capable of achieving excellent nanoparticle dispersion and a narrow size distribution for both Pt/SG (Figure 1a,b) and Pt/G (Figure 1c,d). The X-ray diffraction (XRD) profile displayed the typical Pt fcc peaks with the diffraction pattern of the commercial state of the art Pt/C (TKK) used throughout the present investigation included for comparison (Figure 1e). By applying the Scherrer equation to the Pt(220) peak, average Pt nanoparticle sizes were calculated to be 2.16, 2.42, 2.25 for Pt/SG, Pt/G, and Pt/C, respectively. These values are in close agreement, albeit slightly larger than the calculated average nanoparticle sizes based on transmission electron microscopy (TEM) image measurements of 2.10, 2.25, and 2.15 nm, respectively.

The Raman spectra for SG and G (Figure 1f) displays a strong D-band peak, typically attributed to disorder or defects in the crystalline graphitic structure of carbon based materials. The ratio of the D-band to G-band ($I_D:I_G$), with the latter attributed to the E_{2g} vibrations from sp² bonded carbon is commonly used as a gauge for structural disorder in graphitic materials. $I_D:I_G$ values for SG and G were calculated to be 1.33 and 0.96, respectively. Although both materials had higher $I_D:I_G$ ratios than those of pristine graphene where the D-band is theoretically non-existent.^[44] Typically, good Pt nanoparticle distribution and uniform sizing are difficult to achieve on relatively inert graphitic surfaces such as CNTs or graphene^[17] and requires the use of specific pre-treatment or functionalization

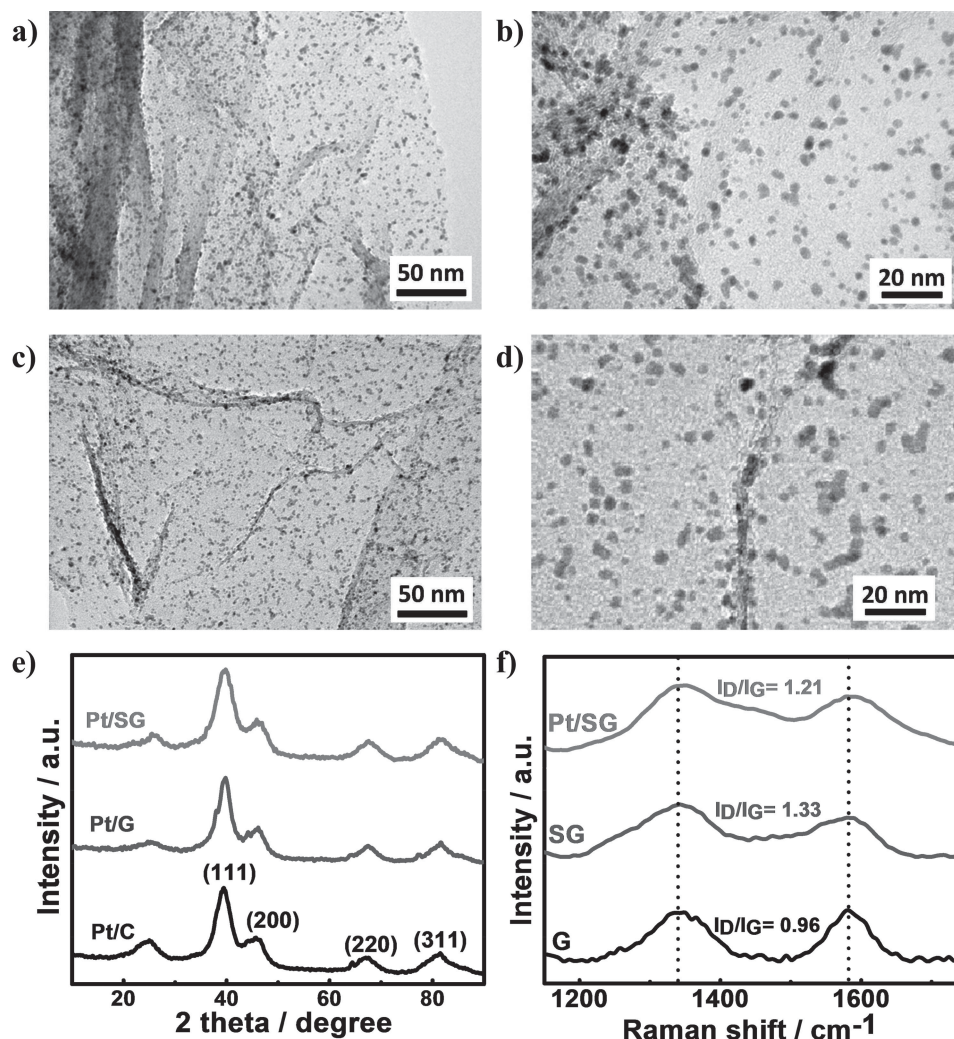


Figure 1. TEM images of a,b) Pt/SG and c,d) Pt/G. e) XRD pattern of Pt/SG, Pt/G, and commercial Pt/C. f) Raman spectra of Pt/SG, SG, and G.

procedures.^[45–47] Clearly the high temperature shock anneal/quench of GO and PDS in the present study is capable of producing graphene-based materials with interruptions in the planar crystal lattice as highlighted by Raman spectroscopy; and furthermore offers reasonable explanation for the facile deposition of well dispersed Pt nanoparticles. This notion is supported by the reduced $I_D:I_G$ ratio of 1.21 for Pt/SG (Figure 1f), suggesting that the Pt nanoparticles deposit favourably on the defect sites of SG, thereby suppressing the vibrations from the underlying functionalities.

To gain understanding of the identity and concentrations of the surface species most likely responsible for the anchorage of Pt catalyst nanoparticles, X-ray photoelectron spectroscopy (XPS) was conducted with the full range spectra displayed in Figure 2a, along with the determined surface atomic concentrations for SG and G provided in Table S1 (Supporting Information) and detailed C1s scan spectra in Figure S3 (Supporting Information). Most noticeably is the appearance of an S2p sulfur signal centered at 161.1 eV for SG, representing a surface concentration of 2.32 at%, a value consistent with results from energy dispersive X-ray (EDX) analysis (2.41 at%, Figure S4,

Supporting Information) that also indicated the sulfur atoms are well distributed throughout the entirety of the materials (Figure S5, Supporting Information). Interestingly, this sulfur content is superior to that of SG materials reported previously^[38–40] and approaching that of a sulfur-doped microporous carbon obtained by heat treating sulfur-rich thienyl-based polymers at the same temperature.^[48] This indicates the effectiveness of applying the thermal shock/quench technique on a mixture of GO and DPS for successfully incorporating sulfur dopants into the final graphene structure.

Figure 2b provides a high resolution XPS scan of the S2p signal deconvoluted into two minor peaks located at 166.69 (peak 1) and 165.51 (peak 2) and two major peaks located at 165.10 (peak 3) and 163.92 eV (peak 4). While the minor peaks can be attributed to carbon bonded SO_x species,^[39,49] the two major peaks appear to result from the S2p spin-orbit doublet ($S2p_{1/2}$ and $S2p_{3/2}$, respectively) with a separation of 1.18 eV, which is in close agreement with the theoretical spin doublet separation of 1.13 eV.^[50] These peaks can be attributed to sulfur bonded directly to the carbon atoms in a heterocyclic configuration^[51,52] as no elemental sulfur was observed by XRD or

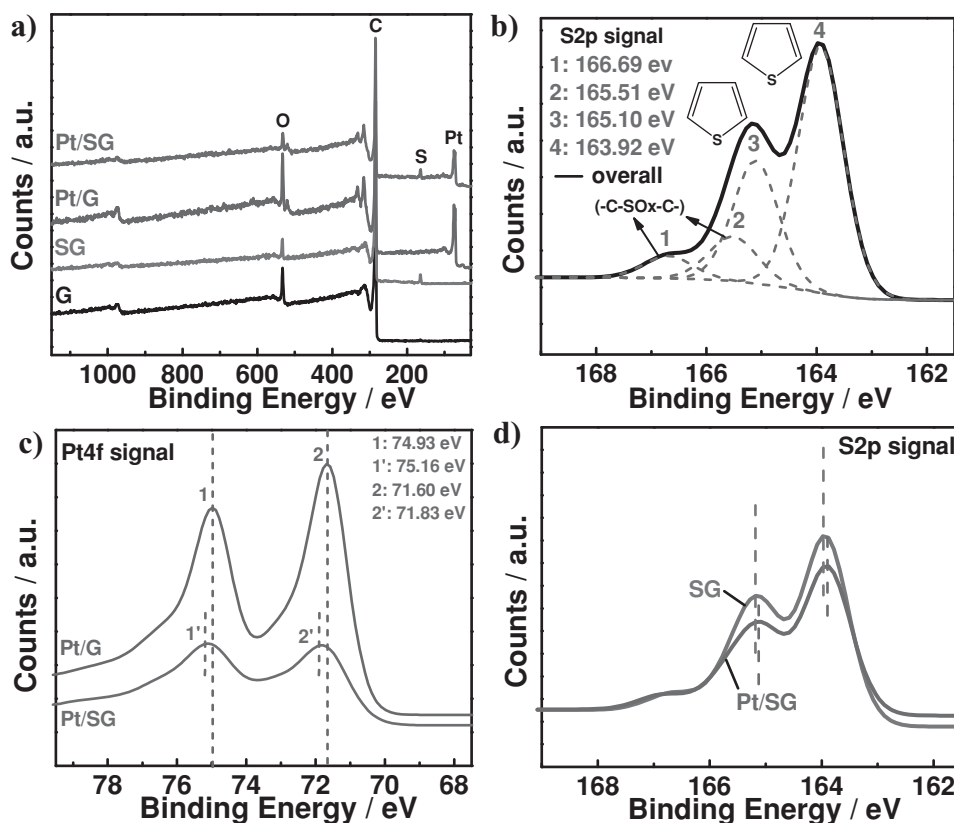


Figure 2. XPS spectra including a) full range spectra for Pt/SG, Pt/G, SG and G, b) S_{2p} spectra of SG, c) Pt_{4f} spectra of Pt/G and Pt/SG, and d) S_{2p} spectra of SG and Pt/SG.

TEM, and (if present) would have been removed by the rigorous washing procedure employed after SG synthesis. We also speculate that these C-S-C species exist in the thiophene form, a notion consistent with previously reported investigations^[38,40,53] and supported by our formation energy calculations discussed later on. Furthermore, thiophene species exist in a pentagonal arrangement, thereby residing on the edge plane and defect sites of SG and most likely giving rise to the strong emergence of the D-band observed through Raman spectroscopy. It is expected that these sulfur based species could serve as anchoring sites for Pt-ion nucleation and subsequent nanoparticle growth.^[41] In terms of Pt deposition on G, well distributed nanoparticles were also obtained most likely anchored on the edge plane or defect sites.^[54] The presence of these moieties in G is indicated through XPS demonstrating a surface oxygen concentration of 7.49 at%, and supported by the collected Raman spectra.

XPS also serves as an important tool for probing the electronic states of catalyst materials, which in the case of Pt plays a governing role in terms of catalyst activity and stability.^[14] Detailed Pt_{4f} spectra are provided in Figure 2c for Pt/G and Pt/SG, whereby both materials display the characteristic doublet of zero-valence Pt^[55] with the Pt_{4f_{7/2}} and Pt_{4f_{5/2}} peaks located at 71.60 and 74.93 eV for Pt/G, and 71.83 and 75.16 eV for Pt/SG, respectively. Small doublet contributions are observed for Pt(II) species at higher binding energies, although the differences between the two samples and contributions to the overall

spectra are difficult to resolve. It is important to notice the positive peak shifts of 0.23 eV for Pt/SG in comparison to Pt/G. This provides indication of an enhanced interaction between the Pt and the support materials, whereby for Pt/SG, the increase in electron binding energy indicates a transfer of electrons from Pt to the SG supports. This notion is further supported by a ca. 0.11 eV negative shift in the S_{2p} doublet peak locations for Pt/SG in comparison to SG, asserting that the sulfur atoms in SG and Pt might exist in a Pt δ^+ -SG δ^- arrangement.^[56]

2.2. Electrochemical Activity and Stability

To investigate catalyst stability, accelerated durability testing (ADT) protocols are commonly employed to simulate the harsh, potentiodynamic and corrosive conditions encountered at the cathode of PEMFCs during operation. Pt/SG, Pt/G and Pt/C catalysts were subjected to 1500 cycles under nitrogen saturated electrolyte with cyclic voltammograms (CVs) collected before and after ADT, as shown in Figure 3a,b and c, respectively. Pt/SG and Pt/G clearly provide higher double layer current densities, attributed to the high surface areas and capacitance capabilities of graphene materials. ECSA values were determined based on the calculated charge for hydrogen adsorption/desorption initially and after each 500 subsequent cycles. It can be seen that the ECSA retention of Pt/SG is clearly superior to that of both Pt/G and commercial Pt/C, retaining 87, 54, and 48%

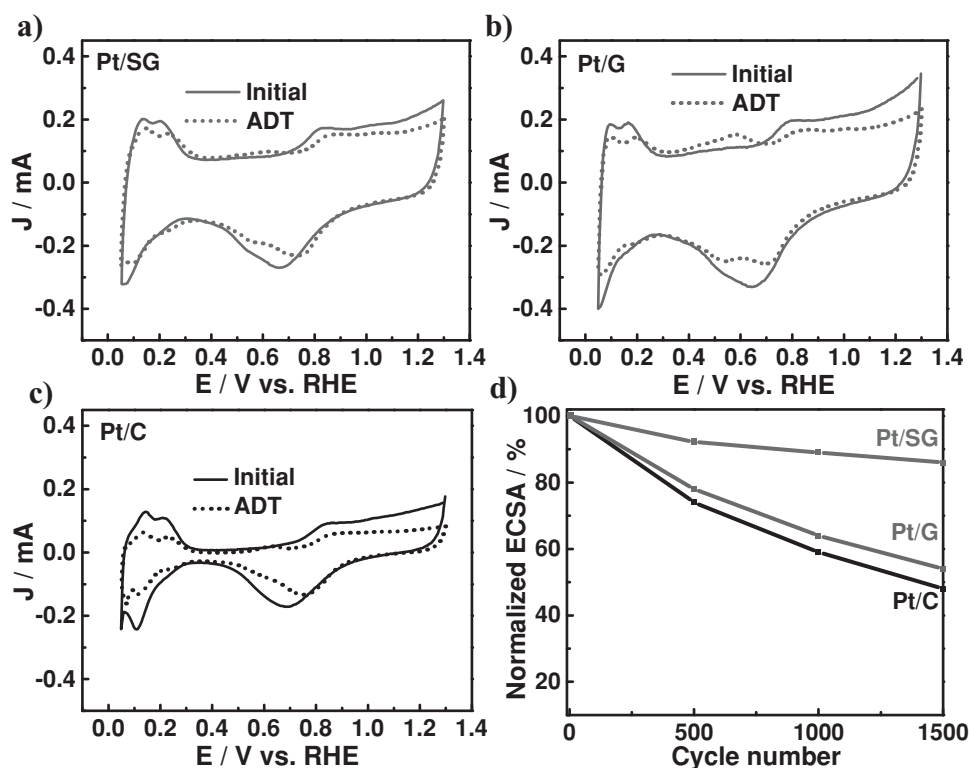


Figure 3. CV curves initially and after ADT for a) Pt/SG, b) Pt/G, c) Pt/C, and d) normalized ECSA remaining throughout ADT.

of their initial surface area after 1500 cycles, respectively. The improved stability of Pt/G in comparison to Pt/C is an observation consistent with previous investigations^[57–59] and primarily attributed to the relatively higher graphitic content of graphene-based supports, enhanced Pt- π orbital bonding strength and the presence of functional anchoring groups. However, the dramatically enhanced stability of Pt/SG in comparison to Pt/C, and more importantly in comparison to Pt/G can be exclusively linked to sulfur incorporation into the graphene structure of the support materials. This strongly suggests that improved catalyst-support interactions between SG and Pt comprise the root cause of these stability enhancements. Interestingly the emergence of quinone/hydroquinone redox peaks (around ≈ 0.6 V vs RHE) were observed after ADT especially in the case of Pt/G. This could be due to the formation of these species, most likely on the planar edges of graphene induced by the high potentials encountered during ADT. In the case of Pt/SG, no suppression of the hydrogen adsorption/desorption peaks or large oxidative currents at potentials above ≈ 1.0 V vs RHE were observed during ADT, indicating that the emission of sulfur-oxide species from SG is not of concern for these developed materials.^[60]

ORR activity polarization curves for Pt/SG, Pt/G and Pt/C were obtained both before and after ADT with results demonstrated in Figure 4a, b and c, respectively. All three materials demonstrate typical ORR polarization curves after correction for electrolyte resistance, with well-defined diffusion limited currents below ≈ 0.7 V vs RHE. Polarization curves at various rotation rates and corresponding Koutecky-Levich plots for Pt/SG are provided in Figure S6 (Supporting Information). It can specifically be seen that Pt/SG initially demonstrates excellent

ORR activity, with a kinetically corrected Pt-mass based activity of $139 \text{ mA mg}_{\text{Pt}}^{-1}$ at an electrode potential of 0.9 V vs RHE (Figure 4d,f) and rotation speed of 1600 rpm. This is superior to that of Pt/G ($101 \text{ mA mg}_{\text{Pt}}^{-1}$) and commercial Pt/C ($121 \text{ mA mg}_{\text{Pt}}^{-1}$) measured under the same conditions at identical Pt electrode loadings. The order of decreasing mass-based activity (Pt/SG > Pt/C > Pt/G) could commensurate with the differences in average Pt nanoparticle size; although as the specific activity of Pt/SG ($279 \mu\text{A cm}^{-2}_{\text{Pt}}$) is superior to that of Pt/G ($235 \mu\text{A cm}^{-2}_{\text{Pt}}$) and Pt/C ($230 \mu\text{A cm}^{-2}_{\text{Pt}}$) despite smaller average nanoparticle sizes, it appears that particular catalyst-support interaction effects are also at play but to an unknown extent.

Pt/SG furthermore possessed excellent ORR activity retention through ADT. After 1500 potential cycles, Pt/SG demonstrated only an 11.2 mV loss in half-wave potential ($E_{1/2}$) and retained almost 78% of the Pt-mass based activity at 0.9 V vs RHE (Figure 4e,f). Meanwhile Pt/G exhibited a 23.0 mV loss in $E_{1/2}$ and retained 56% of its Pt-mass based activity at 0.9 V vs RHE; whereas Pt/C demonstrated a significant $E_{1/2}$ loss of 43.0 mV and retained only 33% of the initial Pt-mass based activity. This consolidates in Pt/SG boasting a 171% higher Pt-mass based activity after ADT in comparison to commercial Pt/C catalyst (108.0 and $39.8 \text{ mA mg}_{\text{Pt}}^{-1}$ at 0.9 V vs RHE, respectively). Once again, and consistent with ECSA loss measurements determined through ADT, Pt/SG displayed the highest stability among the materials investigated, followed by Pt/G and with commercial Pt/C displaying comparatively poor stability.

As Pt particle agglomeration and dissolution are among the primary mechanistic pathways of catalyst degradation and performance loss during PEMFC operation, TEM operates as

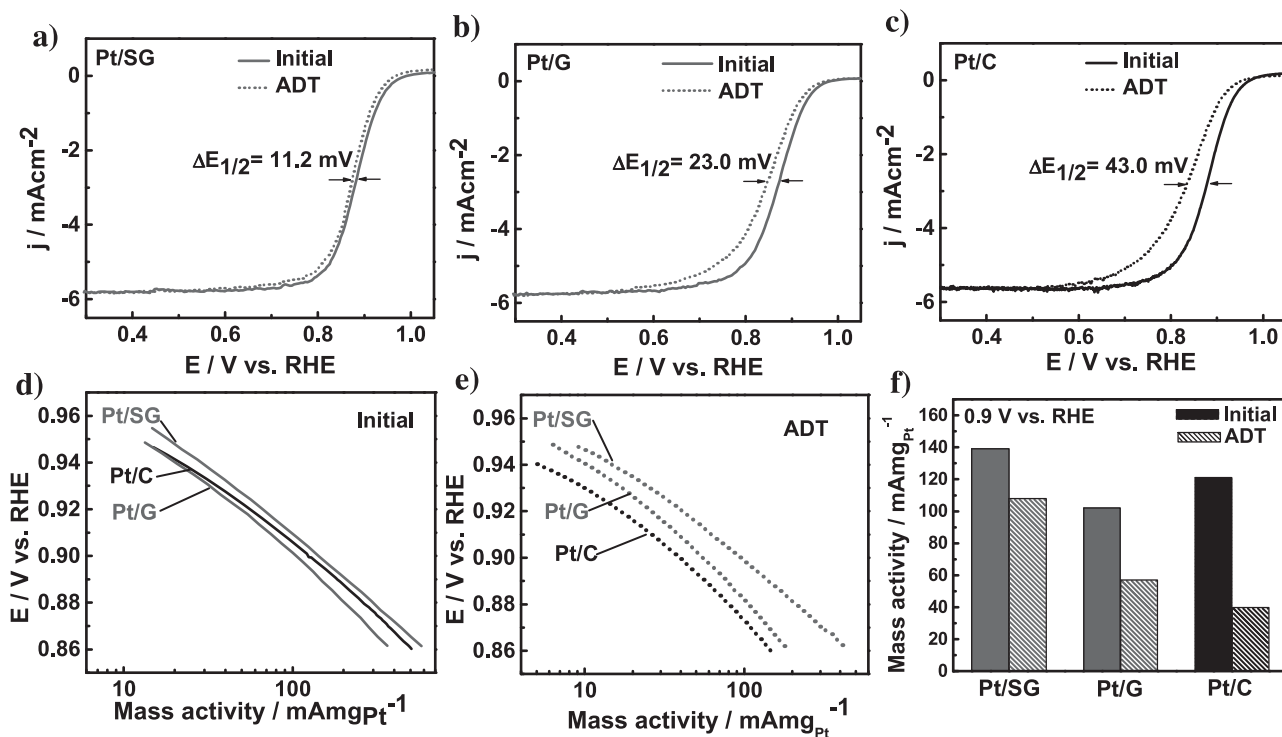


Figure 4. ORR polarization curves initially and after ADT for a) Pt/SG, b) Pt/G, and c) Pt/C. Kinetically controlled Pt mass based activity at low overpotentials d) initially and e) following ADT. f) Kinetically corrected Pt mass based activities of each catalyst before and after ADT.

a powerful tool for investigating the morphological changes occurring in catalyst materials following ADT.^[61,62] Figure 5 provides TEM images and corresponding particle size distributions after ADT for Pt/SG (Figure 5a,b), Pt/G (Figure 5c,d) and Pt/C (Figure 4e,f, with TEM images of as-purchased Pt/C provided in Figure S7, Supporting Information), respectively. Interestingly, Pt/SG still possessed small Pt nanoparticles uniformly distributed across the entirety of the SG support surface (Figure 5a). Notably, based on measurement of over 200 individual nanoparticles (Figure S8, Supporting Information), the average Pt nanoparticle size increased from 2.10 nm to only 2.30 nm. On the other hand, Pt/G (Figure 5c) and Pt/C (Figure 5e) demonstrated more significant nanoparticle growth, with Pt/C demonstrating significantly more noticeable particle agglomeration. Specifically, Pt/G displayed an average Pt nanoparticle size increase from 2.25 to 3.80 nm (Figure 5d), and Pt/C more-so displayed an average size increase from 2.15 to 5.25 nm (Figure 5f). This provides further verification of the beneficial impact of using SG support materials that can suppress the agglomeration and growth of Pt nanoparticles during electrochemical cycling. To further experimentally investigate the interactions occurring between sulfur dopant species in SG and Pt nanoparticles, a select area of Pt/SG following ADT (Figure 5g) was subjected to high-angle annular dark field (HAADF) imaging and EDX colour mapping. ADT on this sample was conducted in the absence of binder in the catalyst ink solution in order to avoid interference from the sulfonate species present in Nafion on sulfur mapping. Figure 5h displays the HAADF image of Pt/SG, with the Pt nanoparticles clearly visible as bright spots distributed the surface of SG.

This image is overlapped with the EDX colour map of Pt/SG in Figure 5i; whereby sulfur species are displayed as green and Pt as red. Clearly the Pt species tend to reside in areas rich in sulfur content, providing indication of the favourable interactions and binding occurring between these species. With experimental results indicating the presence of improved interactions between Pt and SG leading to enhanced ORR activity and electrochemical stability; we turn to computational simulations from a first-principles perspective in order to gain insight into the exact nature of these enhancements.

2.3. Computational Investigations of Sulfur Doping

To investigate and understand the support effects of SG, a 4×4 supercell of graphene (Figure 6a) was selected for the calculations. We assumed that a single carbon atom is replaced by a sulfur atom as shown in Figure 6c and described as “graphitic S”. In addition, thiophene-like sulfur (thiophene S) existing in a pentagonal arrangement was considered by eliminating the carbon atom adjacent to sulfur from the model supercell as illustrated in Figure 6e. The formation energy (E_F) of each structure was calculated by Equation S1, Supporting Information. E_F can be regarded as the additional stability of each structure, indicative of the energetic stability relative to that of a homogeneous local environment at the same concentrations.^[63] E_F values were calculated to be 0.21 and 0.19 eV atom^{-1} for graphitic S and thiophene S, respectively. This provides indication that thiophene S formation is more favourable during SG synthesis, a notion that is supported by the results of XPS analysis

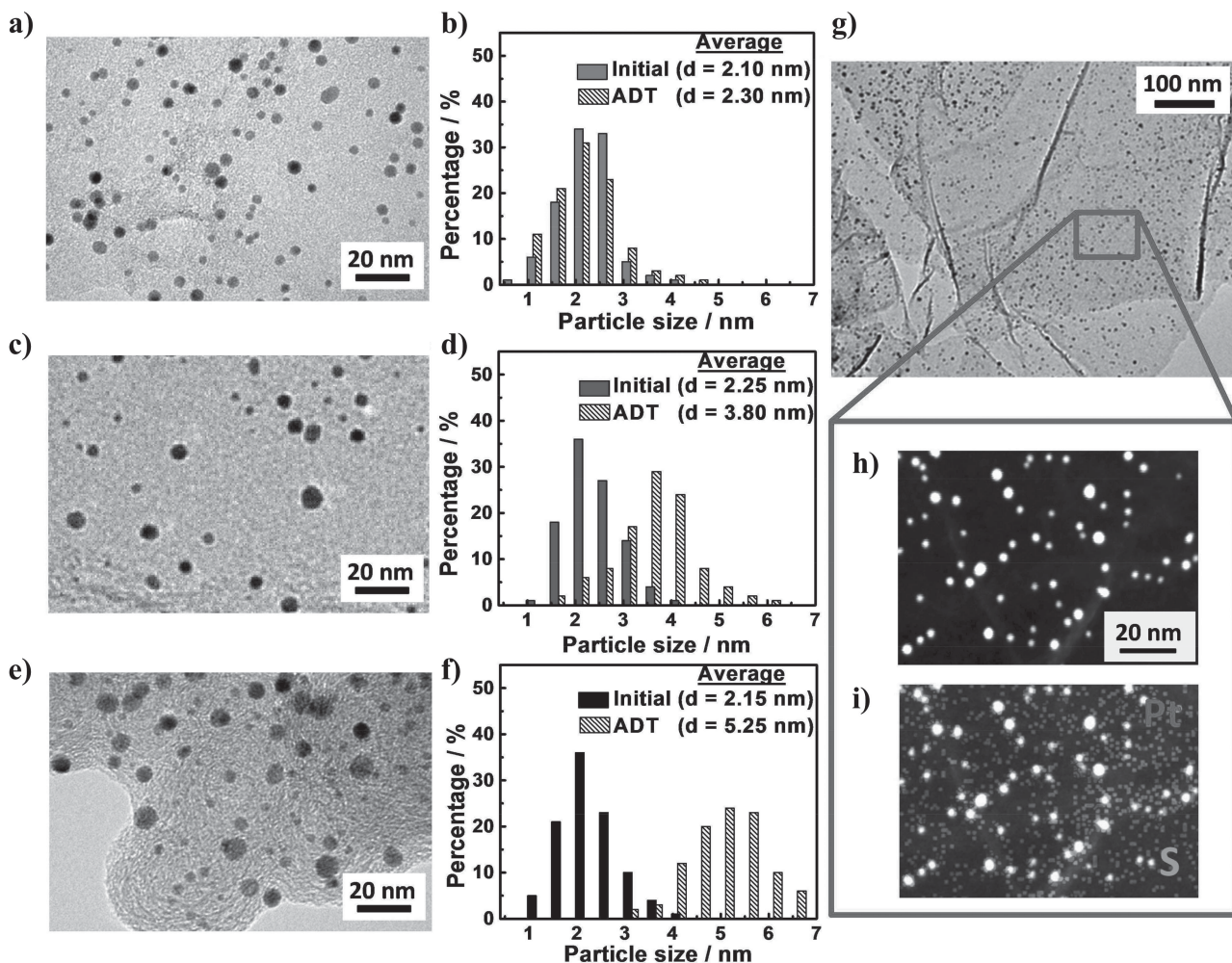


Figure 5. TEM images after ADT and particle size distributions initially and after ADT for a,b) Pt/SG, c,d) Pt/G, and e,f) Pt/C. g) TEM, h) HAADF, and i) overlapped EDX and HAADF image for Pt/SG after ADT.

after high temperature thermal annealing. In the case of pristine graphene, the C–C bond distance is 1.42 Å, which is very close to experimentally measured value of 1.42 Å.^[64] On the other hand, the C–S distance in the model complex was found to change from 1.42 to 1.70 Å for graphitic S doped graphene after relaxation, due to the different atomic radius of sulfur (1.04 Å) in comparison to carbon (0.77 Å). For thiophene S doped graphene, the C–S bond distance was further increased to 1.87 Å.

Previous investigations have linked enhanced catalytic activity and improved metallic nanoparticle dispersion to the modulated electronic structures and chemical properties of graphitic materials induced by heteroatomic doping.^[64–72] Density of states (DOS) and projected density of states (PDOS) analysis can provide insight into these modifications and furthermore allow further understanding regarding the interactions occurring between the surface of graphene and any adsorbed species or reactants.^[64,68,69,72,73] DOS and PDOS were analyzed for the valence electrons of the pristine graphene and sulfur incorporated graphene materials with the results shown in Figure 6. Specifically, Figure 6b displays the

DOS for pristine graphene, demonstrating the conical shape near the Fermi level as consistent with previous reports.^[74–76] Thus, graphene is considered a semi-metal because there is no band gap in addition to no density of electronic states at the Fermi level,^[74] with the electrical conductivity of these materials governed by Dirac's equation.^[76] The substitution of graphitic S into graphene results in a shift of the Fermi level towards higher energies as shown in the PDOS of the carbon atoms and the DOS of these materials as displayed in Figure 6d. Furthermore, for graphitic S doped graphene, the electrons occupy the energy states at the Fermi level, implying excellent electrical conductivity which is an important consideration when dealing with electrode materials.^[77] Interestingly, the position of the Fermi level for thiophene S doped graphene (Figure 6f) is not significantly from that of graphene doped with graphitic S; however there is a band gap generated at the Fermi level which implies that excellent electrical conductivity cannot be expected. Nevertheless, this is not a limiting factor as a support for ORR electrocatalysis because the band gap could be filled after the deposition of Pt atoms onto these materials.

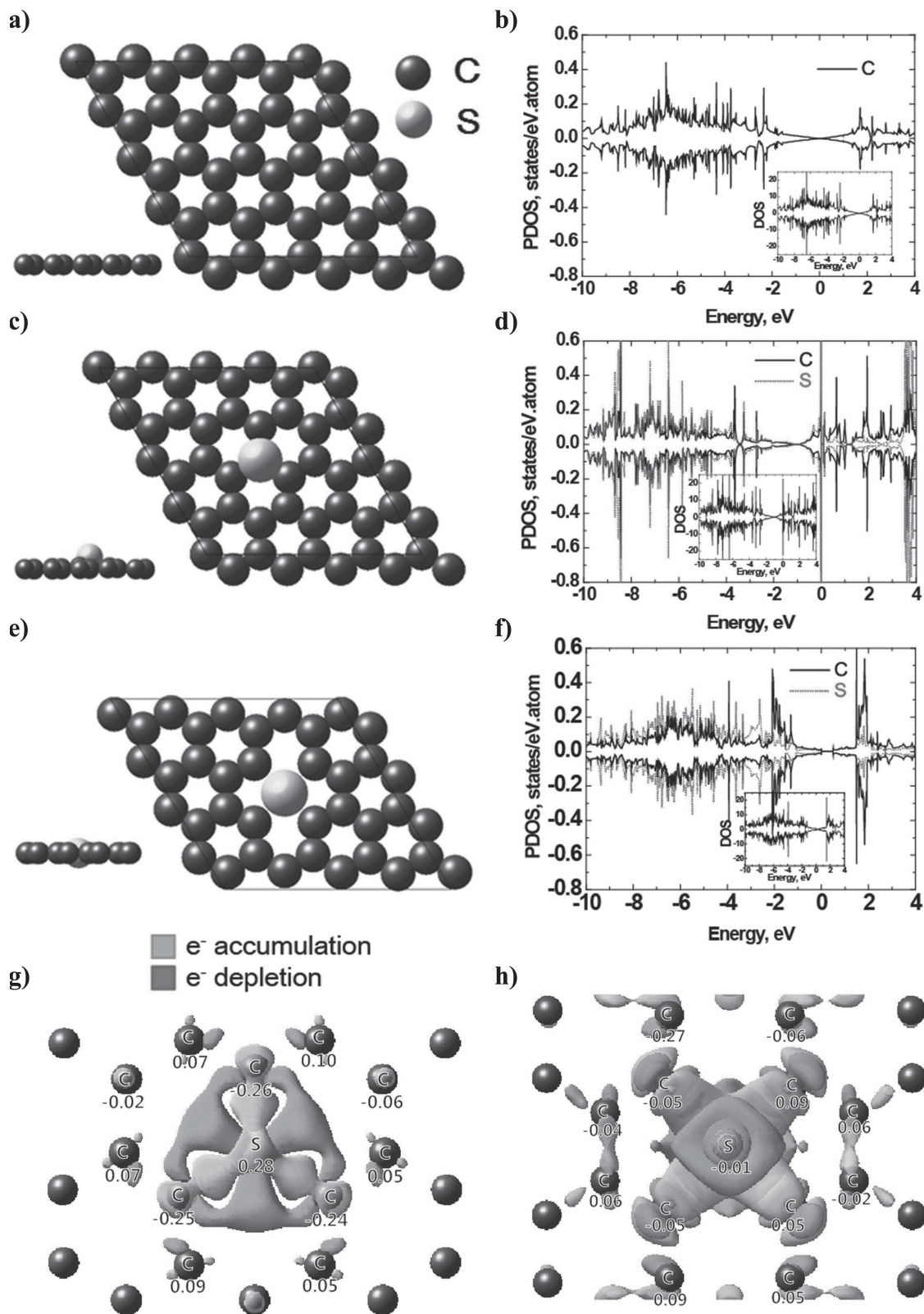


Figure 6. Schematic top views of the model systems and PDOS of a,b) graphene, c,d) graphitic S doped graphene, and e,f) thiophene S doped graphene. Charge density changes of g) graphene and h) thiophene S doped graphene.

The atomic partial charges and changes to the charge density of individual atoms were using Bader charge analysis.^[78] The total number of valence electrons calculated from the Bader charge method are 128, 130 and 126 for a (4 × 4) supercell of pristine graphene, graphitic S and thiophene S doped graphene, respectively. The charge of the graphitic S atom in graphene is depleted to 0.28 e (Figure 6g) whereas the thiophene S atom has accumulated a slight charge of −0.01 e (Figure 6h). Generally electron charge accumulation or depletion is attributed to charge transfer occurring from the atoms with lower electronegativity to atoms with higher electronegativity.^[79–81] However, in the present case the electronegativity of sulfur (2.58) is similar to that of carbon (2.55) on the Pauling scale.^[82] Interestingly, for the graphitic S doped graphene (Figure 6g), the electronic charge of the sulfur atom is depleted towards the neighbouring carbon atoms which possess charge densities varying from −0.24 to −0.26 e. Conversely, the sulfur atom in thiophene S doped graphene has a slight charge accumulation (Figure 6h). Clearly these results indicate that the exact charge transfer phenomena and electronic properties of the SG materials depend on the specific arrangement of the dopant atoms. Regardless, the disruptions of the sp² carbon hybridization caused by heteroatomic sulfur dopants results in a change of the Fermi level and DOS of the materials; modifications that can provide beneficial enhancements to the Pt catalyst-support interactions.

2.4. Electronic Structure Analysis of Pt Atoms on SG

Prior to the investigation of SG supported Pt nanoparticles, the adsorption of a single Pt atom on a (4 × 4) unit cell of pristine

graphene, graphitic S doped graphene and thiophene S doped graphene were investigated to determine how support materials interact with Pt and to obtain and visualize their stable configurations. Each Pt atom was placed on the top, hollow and bridge sites of the three different unit cells to elucidate the most energetically favoured nucleation site, an important determination in order to ensure the reliability of subsequent DFT simulations. After relaxation, it was determined that pristine graphene (Figure 7a) and thiophene S doped graphene (Figure 7c) preferentially adsorb a single Pt atom on the C–C and C–S bridge site, respectively; whereas graphitic S doped graphene (Figure 7b) adsorbs Pt favourably on the top site. In addition, the bond length between the Pt atom and nearest adjacent carbon atom on graphitic S (2.05 Å) and thiophene S (2.06 Å) doped graphene is shorter than that of pristine graphene (2.08 Å); an observation that can likely be related to the adsorption energy between Pt and carbon (E_{ads}) on the support materials that can be calculated by Equation S2, Supporting Information. It has been well established that the interactions occurring between a catalyst material (i.e., Pt) and support play a significant role in the final composite structure in terms of nanoparticle size and distribution because the properties of the support directly affect the nucleation and growth processes during preparation.^[9,83,84] The E_{ads} of Pt on graphitic S and thiophene S doped graphene are −3.27 and −2.68 eV, respectively. These are more negative than that of Pt on pristine graphene (−2.01 eV), highlighting the fact that Pt adsorbs significantly stronger on SG materials as a result of sulfur incorporation. Not only will this enhanced interaction between the Pt and support aid in Pt nanoparticle dispersion and size uniformity as consistent with TEM analysis; the strengthened interactions will provide a tethering

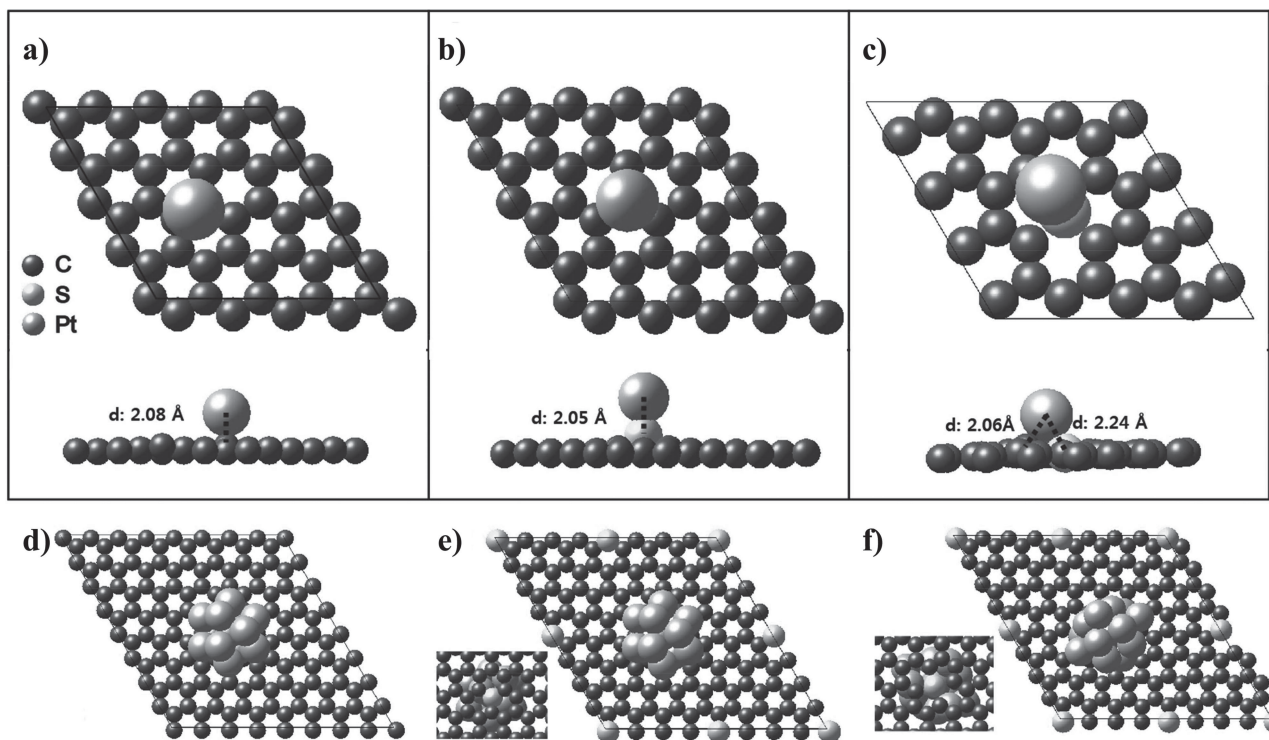


Figure 7. Schematic top and side view of Pt atom adsorption on a) graphene, b) graphitic S doped graphene, and c) thiophene S doped graphene. Schematic top and bottom (inset) views of Pt nanoparticles on d) graphene, e) graphitic S doped graphene, and f) thiophene S doped graphene.

effect between the SG and Pt nanoparticles that can prohibit their self-agglomeration or dissolution under conditions such as those encountered during fuel cell operation.

2.5. Ab-Initio Simulations of Pt Nanoparticles on SG

Prior to the relaxation of graphene supported Pt, free standing icosahedron Pt₁₃ nanoparticles were fully relaxed to find their optimized form under vacuum conditions. Then, the icosahedron Pt nanoparticle is deposited onto pristine graphene (Figure 7d), along with graphitic S (Figure 7e) and thiophene S (Figure 7f) doped graphene for subsequent calculations that will allow us to gain a comprehensive understanding of the previously reported electrocatalyst activity and excellent stability under acidic operating conditions. The d-band center model proposed by Nørskov et al.^[85–91] has turned out to be very useful for describing the underlying mechanisms of experimentally observed, albeit complicated surface catalytic reactions. Using the d-band center model, the electronic structure of the surface exposed metal layer and its inherent catalytic activity can be correlated.^[88] This model relies on the assumption that the weighted average of the d-band electron energies (d-band center) of a catalyst is strongly correlated to the binding energy of the catalyst atoms with the chemical species adsorbed (e.g., oxygen).^[87,88,90,92] Utilizing these underlying fundamentals, Pt alloys with weaker oxygen binding energies than conventional Pt materials have been predicted to possess superior ORR activities by DFT calculations;^[85–87,90,91] an assertion that has further been translated into experimental observations by a variety of researchers employing extended surface and bulk catalysts.^[93–96] In the case of nanoparticles however, intrinsic ORR activity enhancements cannot be exclusively linked to the d-band center theory owing to complications due to the coordination environment and particle size effect of Pt that significantly affects the chemical ability to adsorb oxygen containing species.^[97] Nevertheless, for the present calculations, it is reasonable to quantitatively evaluate the adsorptive strengths of oxygen due to the fact these materials consist of pure Pt with minimal differences in nanoparticle size.^[98] Therefore, the icosahedron Pt₁₃ nanoparticle deposited on G and SG materials was used to calculate the d-band center value and predict variations in ORR activity. From the PDOS of Pt atom, d band center values are evaluated on the graphene based support materials using:^[99]

$$E_d = \frac{\int_{-\infty}^{E_F} E p_d(E) dE}{\int_{-\infty}^{E_F} p_d(E) dE} \quad (1)$$

Here, p_d is the density of states projected onto the d orbitals of a Pt atom. The Pt atoms were selected at vertex site near support, and the d-band center values were calculated to be -2.33 , -2.50 , and -2.72 for graphene, graphitic S, and thiophene S doped graphene, respectively. Independent of the arrangement of sulfur dopants within the SG, the d-band center of the Pt nanoparticle is shifted downward. This observation is even consistent with a previous investigation that indicated a negative d-band

shift for Pt nanoparticle supported on CNTs functionalized with thiol groups; present not necessarily incorporated into the planar graphitic lattice of CNTs, but rather as functional species extending from the basal plane of these supports.^[100] Regardless, the negative shift in the d-band center for the Pt nanoparticles supported on SG is reflected in the improved ORR kinetics of Pt/SG in comparison to Pt/G observed through half-cell experimental investigations.

The Pt nanoparticles are stabilized by a subtle interplay occurring between the size-dependent cohesive energy per atom and the propensity for nanoparticle surface energy minimization.^[101] It has been proposed that lower cohesive energies results in a lowering of the electrochemical dissolution potential of Pt into acidic solutions.^[98,101–103] The cohesive energies of Pt nanoparticles on different support materials (E_{coh}) can be calculated using:

$$E_{coh} = \frac{E_{Pt/support} - E_{support} - nE_{Pt,g}}{n} \quad (2)$$

Here, $E_{Pt,g}$ is the total energy of an individual Pt atom, n is the number of Pt atoms, $E_{Pt/support}$ is the total energy of the support with the Pt cluster adsorbed on it, and $E_{support}$ is the total energy of the support. The cohesive energy of the unsupported Pt₁₃ icosahedron is -3.62 eV taking into consideration spin polarized calculations, a value that is consistent with our previous reports.^[98,101] Supported on graphene based materials, the values of the Pt₁₃ nanoparticles were calculated to be -3.67 , -3.77 , and -3.95 eV for the case of pristine graphene, graphitic S and thiophene S doped graphene, respectively. Clearly the cohesive energy of Pt₁₃ can be increased by employing graphene based support materials. Moreover and most notably, the cohesive energy of the Pt nanoparticles can be increased when using graphene doped with either graphitic or thiophene like sulfur species. This, by extension implies that the electrochemical dissolution potential of Pt nanoparticles supported on SG could be increased. Once again, the result of this computational analysis supports our findings that indicate Pt/SG provides excellent electrochemical stability investigated through ADT protocols in acidic electrolyte.

3. Conclusions

SG materials (2.32 at% S) were prepared by thermally shock/quench annealing a mixture of GO and PBS. The SG materials were used to support well dispersed uniformly sized (≈ 2.10 nm) Pt nanoparticles for ORR catalysis. Pt/SG demonstrated excellent ORR activity based on half-cell investigations, providing a Pt-mass based current of $139 \text{ mA mg}_{Pt}^{-1}$ at an electrode potential of 0.9 V vs RHE . This performance was superior to that of commercial Pt/C ($121 \text{ mA mg}_{Pt}^{-1}$) and Pt/G ($101 \text{ mA mg}_{Pt}^{-1}$); exclusively illustrating the beneficial impact of sulfur dopants in graphene supports. Notably, Pt/SG demonstrated outstanding electrochemical stability through ADT, displaying only an 11.2 mV decrease in ORR half-wave potential and maintaining 87% of its initial ECSA after 1500 potential cycles. This was a dramatic improvement over Pt/G and Pt/C, which demonstrated 23.0 and 43.0 mV losses in

half-wave potential, while retaining only 54 and 48% of their initial ECSA, respectively. Finally, in order to fundamentally investigate the role of catalyst-support interactions for these new materials, computational simulations highlighted that sulfur doping of graphene could provide stronger interactions with Pt and enhanced nanoparticle cohesive energies which was used to explain the outstanding electrochemical stability of Pt/SG. Furthermore, the sulfur dopants modulated the electronic properties of Pt, resulting in a negative shift in the d-band that translated to the enhanced ORR kinetics observed. By effectively coupling experimental and computational investigations, we have exclusively demonstrated that SG materials can be considered an extremely promising new class of catalyst support materials both from an ORR activity and stability standpoint that can significantly advance the current state of PEMFC catalyst technology.

4. Experimental Section

Material Preparation: Detailed experimental procedures are provided in the Supporting Information. Briefly, GO was prepared by a method reported previously by Marcano et al.,^[104] and was doped with sulfur by mixing with PDS (2:1 w/w) and heat treating at 1000 °C by a thermal shock/quench annealing process under argon protection. Pure G was prepared by the same technique in the absence of PDS. Pt was deposited onto SG and G by a modified ethylene glycol technique.^[42]

Electrochemical Activity and Durability Measurements: Glassy carbon electrodes were coated with catalysts at a loading of 20 $\mu\text{g}_{\text{Pt}} \text{cm}^{-2}$ and tested in 0.1 M HClO_4 at 30 °C. Commercial state of the art Pt/C (TKK, 28.2 wt.% Pt) was also tested for comparison. ORR activity was measured at 10 mV s^{-1} under oxygen saturation and background currents obtained under nitrogen saturation were removed to eliminate capacitance contributions. ADT was carried out by cycling the electrode potential under nitrogen saturation 1500 \times between 0.05 and 1.3 V vs RHE at a scan rate of 50 mV s^{-1} .

Computational Simulations: Additional details of the density functional theory calculations that were not provided in the main text are available in the Supporting Information.

Supporting Information

Supporting Information is available from the Wiley Online Library or from the author.

Acknowledgements

D.H. and Md.A.H. contributed equally to this work. This research was conducted as part of the Catalysis Research for Polymer Electrolyte Fuel Cells (CaRPE FC) Network administered from Simon Fraser University and supported by Automotive Partnership Canada (APC) Grant No. APCPJ 417858 – 11 through the Natural Sciences and Engineering Research Council of Canada (NSERC). Additional support was also provided by the Waterloo Institute for Nanotechnology, the University of Waterloo and the Supercomputing Center/Korea Institute of Science and Technology Information with supercomputing resources including technical support (KSC-2013-C2-008). TEM images were obtained at the Canadian Center for Electron Microscopy at McMaster University.

Received: January 16, 2014

Revised: February 14, 2014

Published online: April 1, 2014

- [1] F. Jaouen, E. Proietti, M. Lefevre, R. Chenitz, J.-P. Dodelet, G. Wu, H. T. Chung, C. M. Johnston, P. Zelenay, *Energy Environ. Sci.* **2011**, *4*, 114.
- [2] Z. Chen, D. Higgins, A. Yu, L. Zhang, J. Zhang, *Energy Environ. Sci.* **2011**, *4*, 3167.
- [3] United States Department of Energy: Technical Plan – Fuel Cells, **2012**. Available online at: http://www1.eere.energy.gov/hydrogenandfuelcells/mypp/pdfs/fuel_cells.pdf (accessed: November 2013).
- [4] R. Borup, J. Meyers, B. Pivovar, Y. S. Kim, R. Mukundan, N. Garland, D. Myers, M. Wilson, F. Garzon, D. Wood, *Chem. Rev.* **2007**, *107*, 3904.
- [5] D. C. Higgins, J.-Y. Choi, J. Wu, A. Lopez, Z. Chen, *J. Mater. Chem.* **2012**, *22*, 3727.
- [6] R. S. Hsu, D. Higgins, Z. Chen, *Nanotechnology* **2010**, *21*, 165705.
- [7] Y.-J. Wang, D. P. Wilkinson, J. Zhang, *Chem. Rev.* **2011**, *111*, 7625.
- [8] S.-Y. Huang, P. Ganesan, S. Park, B. N. Popov, *J. Am. Chem. Soc.* **2009**, *131*, 13898.
- [9] Y. Zhou, K. Neyerlin, T. S. Olson, S. Pylypenko, J. Bult, H. N. Dinh, T. Gennett, Z. Shao, R. O'Hayre, *Energy Environ. Sci.* **2010**, *3*, 1437.
- [10] Y. Shao, J. Sui, G. Yin, Y. Gao, *Appl. Catal., B* **2008**, *79*, 89.
- [11] J. Zhou, X. Zhou, X. Sun, R. Li, M. Murphy, Z. Ding, X. Sun, T.-K. Sham, *Chem. Phys. Lett.* **2007**, *437*, 229.
- [12] C. T. Campbell, *Nat. Chem.* **2012**, *4*, 597.
- [13] S. Sharma, B. G. Pollet, *J. Power Sources* **2012**, *208*, 96.
- [14] S. Shrestha, Y. Liu, W. E. Mustain, *Cat. Rev.* **2011**, *53*, 256.
- [15] Y. Sun, Q. Wu, G. Shi, *Energy Environ. Sci.* **2011**, *4*, 1113.
- [16] M. K. Debe, *Nature* **2012**, *486*, 43.
- [17] E. Antolini, *Appl. Catal., B* **2012**, *123–124*, 52.
- [18] D. U. Lee, H. W. Park, D. Higgins, L. Nazar, Z. Chen, *J. Electrochem. Soc.* **2013**, *160*, F910.
- [19] D. Higgins, Z. Chen, D. U. Lee, Z. Chen, *J. Mater. Chem. A* **2013**, *1*, 2639.
- [20] D. Geng, Y. Chen, Y. Li, R. Li, X. Sun, S. Ye, S. Knights, *Energy Environ. Sci.* **2011**, *4*, 760.
- [21] D. Higgins, Z. Chen, Z. Chen, *Electrochim. Acta* **2011**, *56*, 1570.
- [22] D. C. Higgins, J. Wu, W. M. Li, Z. W. Chen, *Electrochim. Acta* **2012**, *59*, 8.
- [23] Z. Chen, D. Higgins, H. Tao, R. S. Hsu, Z. Chen, *J. Phys. Chem. C* **2009**, *113*, 21008.
- [24] K. Gong, F. Du, Z. Xia, M. Durstock, L. Dai, *Science* **2009**, *323*, 760.
- [25] L. Qu, Y. Liu, J.-B. Baek, L. Dai, *ACS Nano* **2010**, *4*, 1321.
- [26] G. Wu, N. H. Mack, W. Gao, S. Ma, R. Zhong, J. Han, J. K. Baldwin, P. Zelenay, *ACS Nano* **2012**, *6*, 9764.
- [27] Y. Chen, J. Wang, H. Liu, M. N. Banis, R. Li, X. Sun, T.-K. Sham, S. Ye, S. Knights, *J. Phys. Chem. C* **2011**, *115*, 3769.
- [28] Y. Chen, J. Wang, H. Liu, R. Li, X. Sun, S. Ye, S. Knights, *Electrochem. Commun.* **2009**, *11*, 2071.
- [29] D. C. Higgins, D. Meza, Z. W. Chen, *J. Phys. Chem. C* **2010**, *114*, 21982.
- [30] R. Imran Jafri, N. Rajalakshmi, S. Ramaprabhu, *J. Mater. Chem.* **2010**, *20*, 7114.
- [31] S. Sun, G. Zhang, Y. Zhong, H. Liu, R. Li, X. Zhou, X. Sun, *Chem. Commun.* **2009**, 7048.
- [32] M. N. Banis, S. Sun, X. Meng, Y. Zhang, Z. Wang, R. Li, M. Cai, T.-K. Sham, X. Sun, *J. Phys. Chem. C* **2013**, *117*, 15457.
- [33] D. Geng, Y. Hu, Y. Li, R. Li, X. Sun, *Electrochem. Commun.* **2012**, *22*, 65.
- [34] Y.-H. Li, T.-H. Hung, C.-W. Chen, *Carbon* **2009**, *47*, 850.
- [35] M. N. Groves, A. S. W. Chan, C. Malardier-Jugroot, M. Jugroot, *Chem. Phys. Lett.* **2009**, *481*, 214.
- [36] M. N. Groves, C. Malardier-Jugroot, M. Jugroot, *J. Phys. Chem. C* **2012**, *116*, 10548.

- [37] T. Holme, Y. Zhou, R. Pasquarelli, R. O'Hayre, *Phys. Chem. Chem. Phys.* **2010**, *12*, 9461.
- [38] J. Liang, Y. Jiao, M. Jaroniec, S. Z. Qiao, *Angew. Chem., Int. Ed.* **2012**, *51*, 11496.
- [39] Z. Yang, Z. Yao, G. F. Li, G. Y. Fang, H. G. Nie, Z. Liu, X. M. Zhou, X. Chen, S. M. Huang, *ACS Nano* **2012**, *6*, 205.
- [40] S. Yang, L. Zhi, K. Tang, X. Feng, J. Maier, K. Müllen, *Adv. Funct. Mater.* **2012**, *22*, 3634.
- [41] R. Wang, D. C. Higgins, M. A. Hoque, D. Lee, F. Hassan, Z. Chen, *Sci. Rep.* **2013**, *3*.
- [42] B. P. Vinayan, R. Nagar, N. Rajalakshmi, S. Ramaprabhu, *Adv. Funct. Mater.* **2012**, *22*, 3519.
- [43] W. Li, X. Wang, Z. Chen, M. Waje, Y. Yan, *J. Phys. Chem. B* **2006**, *110*, 15353.
- [44] A. C. Ferrari, D. M. Basko, *Nat. Nanotechnol.* **2013**, *8*, 235.
- [45] S. M. Choi, M. H. Seo, H. J. Kim, W. B. Kim, *Carbon* **2011**, *49*, 904.
- [46] J.-D. Qiu, G.-C. Wang, R.-P. Liang, X.-H. Xia, H.-W. Yu, *J. Phys. Chem. C* **2011**, *115*, 15639.
- [47] B. Seger, P. V. Kamat, *J. Phys. Chem. C* **2009**, *113*, 7990.
- [48] J. P. Paraknowitsch, A. Thomas, J. Schmidt, *Chem. Commun.* **2011**, *47*, 8283.
- [49] C. H. Choi, S. H. Park, S. I. Woo, *Green Chem.* **2011**, *13*, 406.
- [50] A. Barrie, I. W. Drummond, Q. C. Herd, *J. Electron Spectrosc. Relat. Phenom.* **1974**, *5*, 217.
- [51] M. E. Labib, J. H. Thomas Iii, D. D. Embert, *Carbon* **1984**, *22*, 445.
- [52] Y. Chang, F. Hong, C. He, Q. Zhang, J. Liu, *Adv. Mater.* **2013**, *25*, 4794.
- [53] I. Herrmann, U. I. Kramm, J. Radnik, S. Fiechter, P. Bogdanoff, *J. Electrochem. Soc.* **2009**, *156*, B1283.
- [54] S. Sun, G. Zhang, N. Gauquelin, N. Chen, J. Zhou, S. Yang, W. Chen, X. Meng, D. Geng, M. N. Banis, R. Li, S. Ye, S. Knights, G. A. Botton, T.-K. Sham, X. Sun, *Sci. Rep.* **2013**, *3*, 1775.
- [55] G. Wu, Y.-S. Chen, B.-Q. Xu, *Electrochem. Commun.* **2005**, *7*, 1237.
- [56] R. Ahmadi, M. K. Amini, *Int. J. Hydrogen Energy* **2011**, *36*, 7275.
- [57] D. He, K. Cheng, H. Li, T. Peng, F. Xu, S. Mu, M. Pan, *Langmuir* **2012**, *28*, 3979.
- [58] R. Kou, Y. Shao, D. Wang, M. H. Engelhard, J. H. Kwak, J. Wang, V. V. Viswanathan, C. Wang, Y. Lin, Y. Wang, I. A. Aksay, J. Liu, *Electrochem. Commun.* **2009**, *11*, 954.
- [59] Y. Shao, S. Zhang, C. Wang, Z. Nie, J. Liu, Y. Wang, Y. Lin, *J. Power Sources* **2010**, *195*, 4600.
- [60] J. Fu, M. Hou, C. Du, Z. Shao, B. Yi, *J. Power Sources* **2009**, *187*, 32.
- [61] K. Hartl, M. Hanzlik, M. Arenz, *Energy Environ. Sci.* **2011**, *4*, 234.
- [62] D. C. Higgins, S. Ye, S. Knights, Z. Chen, *Electrochem. Solid-State Lett.* **2012**, *15*, B83.
- [63] B. Han, V. Viswanathan, H. Pitsch, *J. Phys. Chem. C* **2012**, *116*, 6174–6183.
- [64] Y. Okamoto, *Appl. Surf. Sci.* **2009**, *256*, 335.
- [65] E. Cruz-Silva, D. A. Cullen, L. Gu, J. M. Romo-Herrera, E. Muñoz-Sandoval, F. López-Urías, B. G. Sumpter, V. Meunier, J.-C. Charlier, D. J. Smith, H. Terrones, M. Terrones, *ACS Nano* **2008**, *2*, 441.
- [66] E. Cruz-Silva, F. Lopez-Urías, E. Muñoz-Sandoval, B. G. Sumpter, H. Terrones, J. C. Charlier, V. Meunier, M. Terrones, *Nanoscale* **2011**, *3*, 1008.
- [67] M. Endo, T. Hayashi, S.-H. Hong, T. Enoki, M. S. Dresselhaus, *J. Appl. Phys.* **2001**, *90*, 5670.
- [68] H. Kim, K. Lee, S. I. Woo, Y. Jung, *Phys. Chem. Chem. Phys.* **2011**, *13*, 17505.
- [69] K. R. Lee, K. U. Lee, J. W. Lee, B. T. Ahn, S. I. Woo, *Electrochem. Commun.* **2010**, *12*, 1052.
- [70] Z. W. Liu, F. Peng, H. J. Wang, H. Yu, W. X. Zheng, J. Yang, *Angew. Chem. Int. Ed.* **2011**, *123*, 3315.
- [71] B. Shan, K. Cho, *Chem. Phys. Lett.* **2010**, *492*, 131.
- [72] L. Zhang, Z. Xia, *J. Phys. Chem. C* **2011**, *115*, 11170.
- [73] Y. Wang, Y. Shao, D. W. Matson, J. Li, Y. Lin, *ACS Nano* **2010**, *4*, 1790.
- [74] M. I. Katsnelson, *Mater. Today* **2007**, *10*, 20.
- [75] R. Lv, M. Terrones, *Mater. Lett.* **2012**, *78*, 209.
- [76] K. S. Novoselov, A. K. Geim, S. V. Morozov, D. Jiang, M. I. Katsnelson, I. V. Grigorieva, S. V. Dubonos, A. A. Firsov, *Nature* **2004**, *438*, 197.
- [77] S. M. Choi, M. H. Seo, H. J. Kim, W. B. Kim, *Carbon* **2011**, *49*, 904.
- [78] R. F. W. Bader, *Atoms in Molecules: A Quantum Theory*; Oxford University Press, USA **1994**.
- [79] J. H. Kim, S. M. Choi, S. H. Nam, M. H. Seo, S. H. Choi, W. B. Kim, *Appl. Catal. B: Environ.* **2008**, *82*, 89.
- [80] S. Mukerjee, S. Srinivasan, M. P. Soriaga, *J. Electrochem. Soc.* **1995**, *142*, 1409.
- [81] M. H. Seo, S. M. Choi, J. K. Seo, S. H. Noh, W. B. Kim, B. Hana, *Appl. Catal. B: Environ.* **2013**, *129*, 163.
- [82] D. R. Lide, *CRC handbook of chemistry and physics*, 86th ed., CRC Press, Boca Raton, Florida, USA **2005**.
- [83] S. H. Joo, S. J. Choi, I. Oh, J. Kwak, Z. Liu, O. Terasaki, R. Ryoo, *Nature* **2001**, *412*, 169.
- [84] M. H. Seo, S. M. Choi, H. J. Kim, W. B. Kim, *Electrochem. Commun.* **2011**, *13*, 182.
- [85] U. B. Demirci, *J. Power Sources* **2007**, *173*, 11.
- [86] J. Greeley, M. Mavrikakis, *Nat. Mater.* **2004**, *3*, 810.
- [87] J. Greeley, I. E. L. Stephens, A. S. Bondarenko, T. P. Johansson, H. A. Hansen, T. F. Jaramillo, J. Rossmeisl, I. Chorkendorff, J. K. Nørskov, *Nature Chem.* **2009**, *1*, 552.
- [88] B. Hammer, J. K. Nørskov, *Nature* **1995**, *376*, 238.
- [89] B. Hammer, J. K. Nørskov, *Surf. Sci.* **1995**, *343*, 211.
- [90] M. Shao, K. Sasaki, N. S. Marinkovic, L. Zhang, R. R. Adzic, *Electrochem. Commun.* **2007**, *9*, 2848.
- [91] M. H. Shao, T. Huang, P. Liu, J. Zhang, K. Sasaki, M. B. Vukmirovic, R. R. Adzic, *Langmuir* **2006**, *22*, 10409.
- [92] M. H. Shao, P. Liu, J. Zhang, R. R. Adzic, *J. Phys. Chem. B* **2007**, *111*, 6772.
- [93] Z. Chen, M. Waje, W. Li, Y. Yan, *Angew. Chem., Int. Ed.* **2007**, *46*, 4060.
- [94] D. F. van der Vliet, C. Wang, D. Tripkovic, D. Strmcnik, X. F. Zhang, M. K. Debe, R. T. Atanasoski, N. M. Markovic, V. R. Stamenkovic, *Nat. Mater.* **2012**, *11*, 1051.
- [95] C. Wang, M. Chi, D. Liv, D. Strmcnik, D. van der Vliet, G. Wang, V. Komanicky, K.-C. Chang, A. P. Paulikas, D. Tripkovic, J. Pearson, K. L. More, N. M. Markovic, V. R. Stamenkovic, *J. Am. Chem. Soc.* **2011**, *133*, 14396.
- [96] H. Zhu, S. Zhang, S. Guo, D. Su, S. Sun, *J. Am. Chem. Soc.* **2013**, *135*, 7130.
- [97] B. C. Han, C. R. Miranda, G. Ceder, *Phys. Rev. B* **2008**, *77*, 75410.
- [98] S. H. Noh, M. H. Seo, J. K. Seo, P. Fischer, B. C. Han, *Nanoscale* **2013**, *5*, 8625.
- [99] P. Kratzer, B. Hammer, J. K. Nørskov, *J. Chem. Phys.* **1996**, *105*, 5595.
- [100] L. Li, S. G. Chen, Z. D. Wei, X. Q. Qi, M. R. Xia, Y. Q. Wang, *Phys. Chem. Chem. Phys.* **2012**, *14*, 16581.
- [101] J. K. Seo, A. Khetan, M. H. Seo, H. Kim, B. Han, *J. Power Sources* **2013**, *238*, 137.
- [102] W. H. Qi, M. P. Wang, *J. Mater. Sci. Lett.* **2002**, *21*, 1743.
- [103] L. Tang, B. Han, K. Persson, C. Friesen, T. He, K. Sieradzki, G. Ceder, *J. Am. Chem. Soc.* **2010**, *132*, 596.
- [104] D. C. Marcano, D. V. Kosynkin, J. M. Berlin, A. Sinitskii, Z. Z. Sun, A. Slesarev, L. B. Alemany, W. Lu, J. M. Tour, *ACS Nano* **2010**, *4*, 4806.